Comptes Rendus

Mécanique

Silvère Akamatsu, Sabine Bottin-Rousseau, Melis Şerefoğlu, Victor T. Witusiewicz, Ulrike Hecht and Mathis Plapp

In situ experiments in microgravity and phase-field simulations of the lamellar-to-rod transition during eutectic growth

Physical Science in Microgravity within the Thematic Group Fundamental and Applied Microgravity / *Sciences physiques en microgravité au sein du GDR Micropesanteur Fondamentale et Appliquée*

In situ experiments in microgravity and phase-field simulations of the lamellar-to-rod transition during eutectic growth

Silvère Akamatsu [a], **Sabine Bottin-Rousseau** [a], **Melis Şerefoğlu** [b], **Victor T. Witusiewicz** [c], **Ulrike Hecht** [c] and **Mathis Plapp**[*, d]

[a] Sorbonne Université, CNRS-UMR 7588, Institut des NanoSciences de Paris, case courrier 840, 4 place Jussieu, 75252 Paris Cedex 05, France

[b] Department of Metallurgical and Materials Engineering, Marmara University, Maltepe, İstanbul, Turkey

[c] Access e.V., Intzestr. 5, 52072 Aachen, Germany

[d] Laboratoire de Physique de la Matière Condensée, CNRS, Ecole Polytechnique, Institut Polytechnique de Paris, 91120 Palaiseau, France

E-mails: silvere.akamatsu@insp.jussieu.fr (S. Akamatsu), bottin@insp.jussieu.fr (S. Bottin-Rousseau), mserefoglukaya@gmail.com (M. Şerefoğlu), v.vitusevych@access-technology.de (V. T. Witusiewicz), u.hecht@access-technology.de (U. Hecht), mathis.plapp@polytechnique.edu (M. Plapp)

Abstract. In recent experiments on the solidification of the binary eutectic alloy succinonitrile-(D)camphor carried out on board of the International Space Station (ISS), a transition from rod to lamellar patterns was observed for low growth velocities. The transition was interpreted in terms of a competition between a propagative instability of lamellae and a drift induced by a transverse temperature gradient. Phase-field simulations of a symmetric model alloy support this scenario: for a fixed transverse temperature gradient, the transition from rods to lamellae occurs for a critical composition at fixed velocity, and for a critical velocity at fixed composition. Since the alloy and control parameters used in experiments and simulations are different, our results strongly suggest that this morphological transition is generic for eutectic alloys.

Keywords. Solidification, Eutectic alloys, In situ experiments, Modeling, Microgravity, Pattern formation.

Published online: 8 February 2023

---

* Corresponding author.

1. Introduction

Experiments on crystal growth and solidification in microgravity have a long tradition [1–12]. The main reason is that the growth of any crystal from melt or solution is accompanied by concentration and/or temperature gradients, and, on ground, the concomitant density gradients create convective motion of the fluid. This complicates the analysis of the growth process and makes a precise control of the growth conditions difficult. Experiments in reduced gravity thus offer a unique possibility to obtain data which can be compared to theories and mathematical models without convection. Examples of such studies in solidification science include benchmark data on dendritic and cellular growth in dilute binary alloys [1,9,10], as well as experiments on eutectic solidification [12].

In addition to such "planned" benchmark data, microgravity experiments can also reveal new effects that would be masked by convection under terrestrial conditions. One example is the recent observation of oscillatory growth modes in cellular solidification [9] that were predicted by numerical simulations [13], but never observed in experiments under terrestrial conditions. In the present contribution, we report on another phenomenon that is difficult to observe on the ground in large samples: the transition from lamellar to rod eutectic growth upon a change of solidification velocity.

A binary eutectic alloy exhibits a temperature T_E in its phase diagram at which the liquid can be in equilibrium with two distinct solids of different compositions. Alloys with a composition sufficiently close to the concentration C_E of the eutectic liquid directly freeze into a two-phase solid. The volume fractions of the two solid phases are approximately fixed by thermodynamics through the lever rule. The spatial organization of the two phases in the bulk solid results from a spontaneous pattern-formation process at the solid-liquid interface. An interplay between diffusion of chemical species in the liquid and capillary effects leads to the emergence of various coupled-growth patterns.
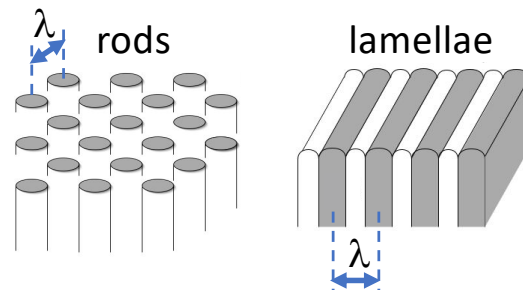

Figure 1. Rod-like and lamellar patterns (schematics). λ: interphase spacing.

The most common coupled-growth patterns are alternating lamellae of the two phases, and rods of the minority phase in a matrix of the majority phase. They are typically obtained during directional solidification, that is, by pulling an alloy sample toward the cold part of a fixed temperature gradient at a fixed velocity V. The standard theory of eutectic growth, formulated by Jackson and Hunt [14], predicts that the characteristic length scale of both lamellae and rods, λ_{JH}, varies as the geometric mean of the diffusion length $l_D = D/V$ (where D is the chemical diffusion coefficient in the liquid), and the capillary length d_0, which is proportional to the surface energy of the solid-liquid interfaces. As a consequence, the product $\lambda_{JH}^2 V$ is constant. It is also commonly stated that lamellae are favored over rods if the volume fractions of the two phases are comparable, whereas rods form for strongly different volume fractions. In this context, the

two relevant variables that control eutectic morphologies are the concentration and the scaled spacing $\Lambda = \lambda/\lambda_{JH}$. Previous studies of morphologies and instabilities have been analyzed in terms of these quantities [15–20].

The above considerations also imply that a dynamic transition between lamellae and rods is expected only when the volume fraction of the solid phases changes with space and/or time, as could indeed happen in the presence of macrosegregation [21]. Such a transition has been observed in phase-field simulations in which the average concentration can be controlled at will [20].

It came thus as a great surprise that a transition from rods to lamellae was observed both in microgravity and ground experiments after a velocity jump [22, 23]. Indeed, according to the scaling theory outlined above, a change of the velocity should change the overall scaling length, but not the morphology.

A tentative explanation of this observation had to take into account several known facts. First, in phase-field simulations it was observed that the transition from lamellae to rods proceeds in a propagative manner: the instability starts at lamella terminations, and one rod after another "pinches off" from the lamella [20]. Second, directional solidification experiments often present a residual transverse temperature gradient which makes the patterns drift laterally when observed along the growth direction [24]. The transition between morphologies could therefore result from the balance between a propagative instability and a lateral drift of the microstructures.

Here, we present the experimental data together with preliminary phase-field simulations which support this scenario. The simulations are carried out for various compositions, transverse temperature gradients, and velocities, and it is shown that a transition from rods to lamellae can be triggered both by increasing the volume fraction of the minority phase, and by lowering the velocity. Whereas no quantitative agreement between experiments and simulations is reached, the simulation data clearly bear out the proposed scenario for the lamella-to-rod transition.

The remainder of this article is structured as follows: we first present the experimental observations made with the Transparent Alloys (TA) apparatus onboard the International Space Station (ISS) in section 2. Then, we outline the tentative interpretation of these observations in section 3. Results of phase-field simulations are presented in section 4, followed by conclusions in section 5.

2. Experiments

2.1. *Methods*

The succinonitrile-(d)camphor (SCN-DC) system (T_E = 38.3 °C; C_E = 13.9 mol%) [25] is a well-known model transparent eutectic alloy for in situ solidification studies [26–29]. It solidifies into nearly pure SCN and DC crystal phases that grow nonfaceted from the melt. The small volume phase fraction of the DC solid phase $\eta \approx 0.24$ favors the formation of DC rods in an SCN matrix. The constant $\lambda_{JH}^2 V = 10.2 \pm 1.5 \ \mu m^3 s^{-1}$ has been estimated in Ref. [27]. Eutectic alloys were prepared with purified SCN and DC. For microgravity experiments, the alloy was contained in a rectangular cartridge with optically flat fused-silica walls (Hellma). We shall define an **xyz** reference frame with **z** being the main solidification axis, **x** the lateral axis parallel to the isotherms, and **y** the transverse axis perpendicular to **x** and **z**. The useful-space dimensions of the samples were 6 mm along **x**, 1 mm along **y** (sample thickness), and 70 mm along **z**.

The TA apparatus (Qinetiq Space, Antverp, Belgium) was designed under the supervision of the European Space Agency (ESA), based on the same method as that presented in Ref. [30]. It has been installed in the Microgravity Science Glovebox (MSG) facility onboard the ISS. The TA setup permits to impose an axial temperature gradient G of about 50 ± 10 Kcm^{-1} in the region of the growth front for regular directional solidification (DS), and to control a transverse gradient

so that the isotherms could be tixted about the **x** axis (tilted-DS configuration; Fig. 2). The tilt angle ϕ was actually set to -6.2 ± 0.3^o. With no tilt ($\phi = 0$), the two straight (when averaged over a long distance) contact lines of the solid-liquid interface with the sample walls (those lines are parallel to the **x** axis) are located at the same z coordinate. By setting $\phi \neq 0$, those two lines remain parallel to each other, but their **z** positions are different. The term of "foremost contact line" will designate the contact line that lies at the larger z value. For solidification, the sample was pulled at a well-controlled velocity V (between 0.007 and 0.04 μms^{-1}) along **z** toward the cold part. Real-time observation was performed from the exterior with a long-distance optics at a fixed, oblique incidence (in the **xz** plane), with an oblique-view angle θ_{opt} set to 43.6 ± 0.3^o about **y**. The optical system delivers dark-field images of the solidification pattern with sharp contrast between the bright DC phase and the dark SCN matrix [30]. Astigmatism due to plane diopters was partly corrected (Lambda-X, Nivelles, Belgium). With the help of elementary numerical processing, good-quality images with a 1:1 aspect ratio were obtained over about 2/3 of the sample thickness. During microgravity experiments, partially automatized TA operations were remotely controlled by telescience from the operation center (E-USOC, Madrid, Spain). Experiments were carried out following a standard protocol: partial directional melting; directional solidification at constant velocity during long period of times (thus reaching a steady-state regime) separated by stepwise V changes (or "jumps"). Morphological changes over time scales ranging from a few minutes to tens of hours were monitored continually. Importantly, no convection motion was observed in the liquid. More technical details can be found in Ref. [22], and references therein.
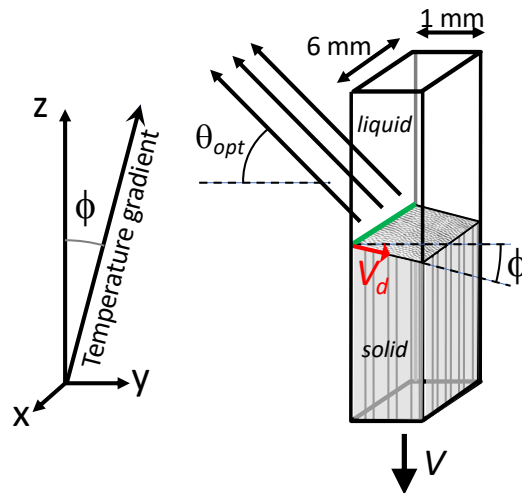

Figure 2. Principle of the tilted-DS method. In green: foremost contact line. Red arrow: drifting direction of the coupled-growth pattern. Symbols: see text.

2.2. *Results*

In order to obtain reference observations in a microgravity environment, regular-DS experiments –that is, with no measurable tilt of the isotherms– were performed. A decreasing-velocity program was operated, starting with $V = 0.04$ μms^{-1}, and ending with $V = 0.007$ μms^{-1}. The alloy was solidified for about 150 hours at the latter velocity. Rod-like patterns made of domains with local hexagonal order, separated by topological defects were observed over the explored V range, in

agreement with previous observations on ground [28, 29]. In practice, after a downward velocity jump, many rods were eliminated (the average spacing was below the rod elimination threshold). At constant velocity, a slow transverse stretching of the pattern, hence a continual increase of the rod spacing, was observed. It was due to a slight forward curvature of the envelope of the growth front (mean radius of curvature: 9-10 mm). This instrumental effect is determined by a deformation of the isotherms, which originates from the different thermal conductivities of the media in presence (glass walls, liquid and solid alloy), both on ground [28], and in microgravity [22]. At long times, the increase of the rod spacing was eventually balanced by rod splitting events. The quasi steady-state distribution of the spacing then roughly extended between the rod elimination threshold λ_{el} on the low-λ side, and the rod-splitting threshold λ_{sp} on the large-λ side. The average spacing λ_{av} was close to λ_{JH}. The stretching effect also provoked a progressive alignment of the hexagons, mostly with dense rows tending to align parallel or perpendicular to the sample walls. Short lamellae were observed at the lowest velocity, close to subboundaries, and in contact with the sample wall (Fig. 3a).
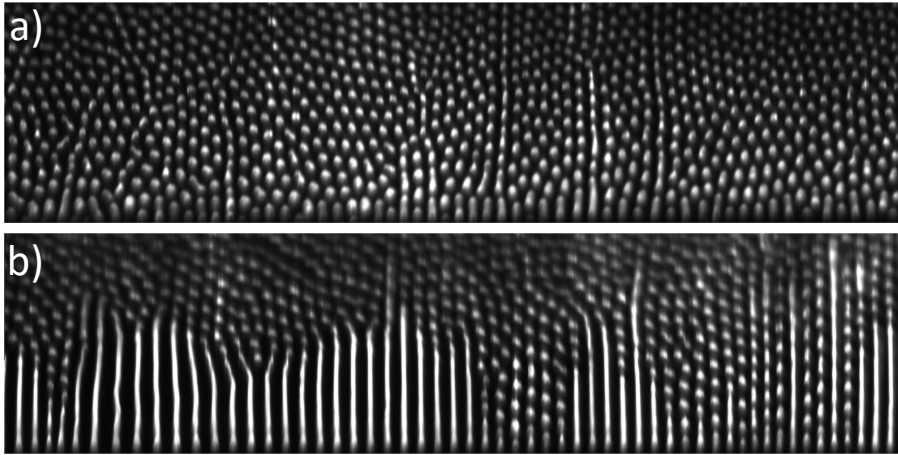

Figure 3. Coupled-growth patterns (eutectic SCN-DC alloy) during DS experiments in microgravity at a low pulling velocity ($V = 0.007\ \mu\mathrm{ms}^{-1}$). a) Regular DS. b) Tilted-isotherm DS. The foremost contact line with the sample wall is at the bottom of the image. Vertical dimension: 500 μm (the upper part of the image was slightly off focus, and is not shown here).

Using the tilted-isotherm configuration, with a fixed inclination of the main axis of the temperature gradient by an angle ϕ from the axis $\mathbf{z}$, a global drift of the coupled-growth pattern was imposed along the transverse direction $\mathbf{y}$. That tilted-DS strategy was used in a previous study (with another transparent eutectic alloy) to propagate a periodic lamellar pattern at the expense of a labyrinth-like pattern [24]. Here, a similar effect – a lateral drift of the pattern – permitted to establish a long-lived coexistence between a pre-existing rod-like pattern and a fresh lamellar domain. Let us review the main stage of that process. We measured the global drift velocity V_d, and confirmed that its component along the $\mathbf{y}$ axis was approximately equal to $V \tan\phi$, according to the geometry of the system, with the rods growing essentially perpendicular to the average front envelope. New rods appeared by splitting at the foremost contact line (Fig. 2). At $V = 0.04\ \mu\mathrm{ms}^{-1}$, no lamellae formed. An efficient alignment of the hexagon domains normal to the sample walls was observed. Long lamellae were observed at low velocity ($V = 0.007\ \mu\mathrm{ms}^{-1}$) after relatively long rod-elimination transient, during which the alignment of the hexagons in the

initial situation was, however, essentially preserved. At that velocity, short, wavy lamellae in the core of the pattern were unstable, breaking up into rods on both ends before reaching a length larger than, say, two or three times the inter-rod spacing in the surrounding pattern. In contrast, straight lamellae that appeared at the foremost contact line were observed to elongate perpendicular to the sample wall. The longest ones were reaching about 500 μm at the ending time of the experiment. A large, stable lamellar pattern was thus growing at the expense of the initial rod-like pattern. This experiment provides, in other words, a clear evidence of a coexistence of dynamically metastable rod-like and lamellar patterns in the form of large domains with uniform morphological features – in contrast to mixed, transient patterns observed previously in directionally solidified eutectic alloys in bulk containers [21, 31, 32] and in confined-geometry samples [33].
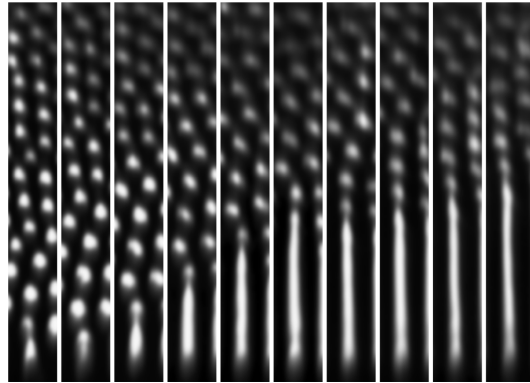

Figure 4. Series of ten successive snapshots showing the time evolution (from left to right) of a single lamella (detail). Same experiment as in Fig. 3b. Time interval between the images: 9 hours 36 minutes. Horizontal dimension of each panel: 60 μm.

Remarkably, the growth rate of the lamellar domain was significantly slower than V_d. The mechanism at play is illustrated in Fig. 4, which shows the evolution of a single lamella within the domain. It can be seen that the lamella formed via the elongation of a rod that was initially located at the foremost contact line. In the first stages, the rod elongated and split several times, until it started to elongate more durably. From that moment, the end of the new lamella in contact with the sample wall remained stable over the whole duration of the experiment. In contrast, the free end (or termination) underwent a repeated breakup, thus emitting new rods that drifted at the velocity V_d once included in the surrounded hexagon pattern. Each breakup event was preceded, and followed by an undulating instability. This scenario is schematically represented in Fig. 5.

3. Tentative interpretation

The experimental observations reported above, together with the results of previous numerical simulations, indicate a possible scenario for the transition from a rod to a lamellar pattern. The "natural" pattern is rod-like, in the sense that the evolution of an extended system from a "random" (that is, largely uncontrolled) initial state of the crystallization front will produce a rod pattern. In the presence of a transverse temperature gradient, lamellae can then grow starting at the sample wall. Such lamellae are subject to two antagonistic effects: (i) the drift induced by the misalignment between the temperature gradient and the sample wall, together with the fact that the lamellae remain "anchored" to the sample wall, leads to an elongation of the lamellae, and (ii) the pinch-off instability at the lamella termination leads to the creation of new rods and thus to a
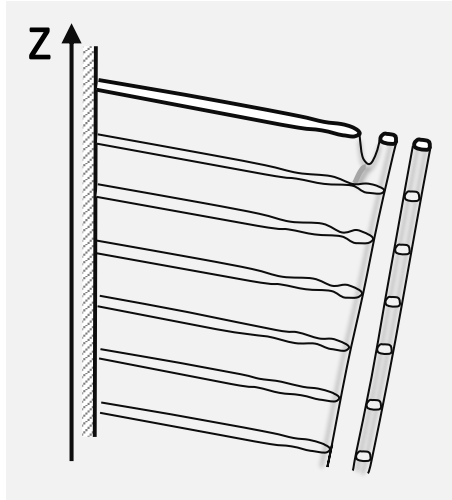
Figure 5. Scheme of the competition between lateral drift and propagating breakup of a lamella of the minority phase. The newly formed rod grows along the direction of the temperature gradient, which is tilted with respect to the sample wall.

shortening of the lamella. If the drift velocity is larger than the propagation velocity of the lamella breakup, the lamellae grow, and could fill the entire system if the duration of the experiment was long enough. In the opposite case, the lamellae can never grow to an appreciable size.

The crucial point is therefore the comparison between the drift velocity and the propagation velocity of the lamella breakup instability. Whereas the former can be linked to the structure of the thermal field, the latter is an intrinsic property of the eutectic system and cannot easily be determined. In the following section, we report on preliminary phase-field simulations which shed some light on this point.

4. Phase-field simulations

We performed three-dimensional phase-field simulations using the model developed in Ref. [34] and the code that has been used in previous simulations of eutectic systems [19, 20, 24, 35]. Our first goal is to confirm the scenario outlined above, and to investigate whether it is generic. For this purpose, it is advantageous to choose alloy and control parameters that lead to efficient numerical calculations, without seeking to reproduce quantitatively the SCN-DC system.

As in previous studies, we use a phase diagram that is completely symmetric with respect to an exchange of the two solid phases α and β, and which has parallel liquidus and solidus lines for the solid-liquid equilibria, and vertical solvus lines. We use a scaled composition variable $c = C - C_E/(C_\beta - C_\alpha)$, where C_E, C_α, and C_β are the concentrations of the liquid and the two solid phases at the eutectic temperature T_E. The nominal volume fractions of the two solid phases are related to the initial composition of the liquid c_0 by $\eta_\alpha = 0.5 - c_0$ and $\eta_\beta = 0.5 + c_0$. As usual, we define three characteristic lengths: the diffusion length $l_D = D/V$, the thermal length $l_T = m\Delta C/G$, and the capillary length $d_0 = \gamma T_E/(L|m|\Delta C)$, with γ the solid-liquid surface free energy (assumed equal for both solid-liquid interfaces), L the latent heat, m the liquidus slope, and $\Delta C = C_\beta - C_\alpha$. The characteristic spacing $\lambda_{JH} \sim \sqrt{l_D d_0}$. The spatial resolution of the phase-field model is set by the thickness W of the diffuse interfaces. We fixed the ratio $l_T/d_0 = 4000$ and simulated two different velocities, corresponding to $l_D/d_0 = 1000$ and $l_D/d_0 = 2000$, respectively;

in the following, we will refer to these two sets as the "fast" and the "slow" velocities. The interface thickness was set to $W/d_0 = 10.826$; this yields $\lambda_{JH} \approx 20\ W$ and $\lambda_{JH} \approx 30\ W$ for the fast and slow velocities, respectively, which is in the range where the phase-field model is well converged. A multi-grid algorithm was employed to achieve both a good resolution of the interface and an efficient treatment of the long-range diffusion field; the grid spacing in the interface region was chosen as $\Delta x = 0.8\ W$. Growth with a transverse temperature gradient is simulated by choosing the thermal field

$$T(x, y, z, t) = T_E + G\left(z + y\sin\phi - Vt\right),\tag{1}$$

where $z = 0$ is defined by the position of the eutectic isotherm at the colder side of the sample ($y = 0$) at $t = 0$. The simulation is started with a disordered initial condition, that is, a solid that is a random mixture of domains in a proportion that corresponds to the lever rule.
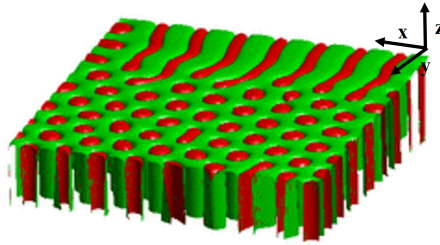

Figure 6. Three-dimensional view of a mixed pattern for $c_0 = 0.16$ and $\phi = 4°$.

Without a transverse temperature gradient ($\phi = 0$), the simulations yield disordered rod patterns that evolve slowly in time by local geometric rearrangements. With $\phi \neq 0$, the patterns depend on the liquid composition c_0. A three-dimensional view of the simulation cell (of lateral section $160 \times 160\ W$) for $\phi = 4°$ is shown in Fig. 6. Here, for better viewing, the foremost contact line (at $y = 0$) is at the rear of the image; the global tilt of the eutectic front can clearly be distinguished. Fig. 7 displays top views of the crystallization front for three different compositions ($c_0 = 0.15$, 0.16, and 0.17, respectively) at three different times, all for $\phi = 4°$ and for the faster velocity. The morphology at long times clearly depends on c_0. For $c_0 = 0.15$, lamellae start to grow at the foremost contact line, elongate across the sample, essentially without pinchoff events, and fill the entire sample at the end of the simulation. A zigzag instability occurs, so that the lamella are not straight. Stable zigzag patterns have been observed both in experiments [36] and in simulations [19] when the lamellar spacing exceeds approximately 1.2 λ_{JH}. In the present experiments, zigzag patterns are observed locally as transient structures [22]; their stability in the simulations in Fig. 7 is possibly due to the small sample size. For $c_0 = 0.16$, lamellae start to grow, but pinchoff occurs at their terminations. The balance between drift and pinchoff seems to depend on the local spacing; some parts of the lamellar front advance well while others lag behind. The rods that have been created by pinchoff events form a regular triangular lattice without defects. Finally, for $c_0 = 0.17$, one can distinguish short "pieces" of lamellae at the foremost contact line, but they never grow longer than about one interrod spacing.

Some particular features of the runs, such as the occurrence of the zigzag instability for $c_0 = 0.15$, the fact that certain lamellae are connected to the sample wall whereas others exhibit a gap, or the inhomogeneous dynamics of the lamellar front, certainly depend on the details of the random initial condition. Nevertheless, it is clear that there is a transition between a lamellar and rod final state for $c_0 \approx 0.16$ (which corresponds to $\eta_\alpha \approx 0.34$) for the tilt angle of $\phi = 4°$.

We repeated similar series of runs for the slower velocity. The average interrod and interlamellar spacing was larger, following the $V^{-1/2}$ scaling. However, a clear departure from scaling occurs,
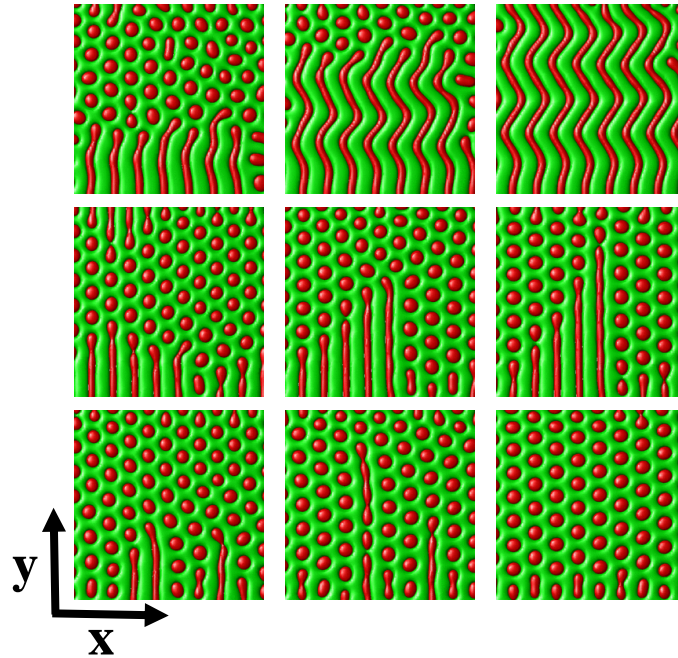
Figure 7. Top views of samples with different composition, at different times. Top row: $c_0 = 0.15$. Middle row: $c_0 = 0.16$. Bottom row: $c_0 = 0.17$. Left, middle and right columns: three times corresponding to solidification distances of 4.8, 9.6 and 14.4 times the lateral system size, respectively. The tilt angle is $\phi = 4°$.

in that the transition between the two morphologies happens for a much lower volume fraction of the minority phase, around $\eta_\alpha \approx 0.25$ ($c_0 \approx 0.25$).

Since the critical volume fraction for the transition from rods to lamellae decreases with decreasing velocity, for a fixed composition (at least in the range between the two critical compositions determined for high and low velocity), there must exist a critical velocity below which the creation of lamellae becomes favored. This is in qualitative agreement with the experimental observations. Furthermore, we performed simulations for different values of the tilt angle. The drift velocity of the rods increased with increasing tilt, and the transition between rods and lamellae occurred for increasing tilt angle at fixed composition and velocity, in agreement with the observations in the experiments of Ref. [22].

The breakup of lamellae can be studied in more detail by performing simulations of single lamellae without a transverse temperature gradient. To this end, a single lamella of spacing 32 W (close to λ_{JH}) is placed in an elongated simulation box with zero-gradient Neumann boundary conditions for all fields on all lateral walls. To trigger the lamella breakup, a small piece of the lamella is removed on one end of the box as illustrated in Fig. 8a; the newly created lamella termination then retracts and forms a round bulbous shape. For $c_0 = 0.26$ (Fig. 8b), this shape remains stationary and no further evolution occurs. For higher concentrations (Figs. 8c, d, and e for $c_0 = 0.27, 0.28$, and 0.29, respectively), successive pinchoff events occur at regular time intervals and create elongated rods. The propagation velocity was determined by dividing the interrod distance by the time interval between pinchoffs; it increases linearly with the distance
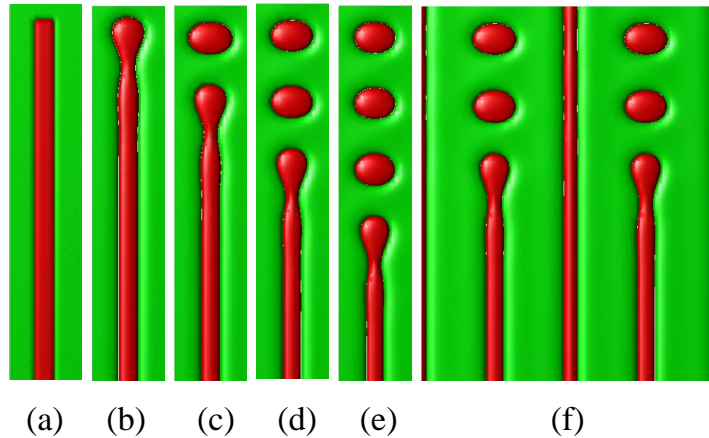
(a)   (b)   (c)   (d)   (e)   (f)

Figure 8. Top views of lamella breakup at the slow velocity without tilt ($\phi = 0°$). (a) initial condition, (b) $c_0 = 0.26$, (c) $c_0 = 0.27$, (d) $c_0 = 0.28$, (e) $c_0 = 0.29$, (f) $c_0 = 0.28$, with neighboring intact lamellae. Snapshots (b) to (f) are all taken after the same solidification distance of 10 lamellar spacings. The lamella termination is stable in (b), whereas lamella breakup is in progress in snapshots (c) to (f).

from the threshold composition ≈ 0.26. A similar transition occurs when the velocity is varied at fixed composition: the lamellar termination is stable below a critical velocity, but unstable above, and the breakup propagation velocity increases linearly with the distance from this velocity threshold.

Since the zero-gradient Neumann boundary conditions are equivalent to a plane of mirror symmetry, the simulations discussed so far correspond to a simultaneous breakup of an infinity of lamellae into a rectangular array of rods. Since such a geometry is never observed in the experiments, we performed several simulations with two lamellae to test the influence of the boundaries on the breakup dynamics. As an example, Fig. 8f shows a simulation cell where the lamella with the termination is placed between two unperturbed lamellae (for a better view of the morphology, two copies of the simulation cell are displayed next to each other). The intact lamellae develops tiny undulations but remain stable, whereas the breakup of the lamella termination proceeds with the same velocity as before.

Besides on velocity and composition, the breakup propagation velocity as well as the critical values for composition and velocity also depend on the lamellar spacing, and possibly on the transverse temperature gradient. For a full quantitative understanding of the morphology transition, these dependencies would need to be studied in detail, but this is outside of the scope of the present work.

5. Conclusion

The results of experiments and phase-field simulations presented here indicate a possible mechanism for the transition from rods to lamellae in directional solidification of eutectic alloys when the velocity is decreased.

The centerpiece of the argument is a competition between the propagative breakup of lamellae and a lateral drift of lamella terminations, starting at one side wall of the sample, which is

driven by a transverse temperature gradient. The phase-field simulations have revealed that for a fixed velocity, there is a critical volume fraction above which the replacement of the rod by a lamellar pattern takes place, and that this critical composition depends on the velocity. As a corollary, for a fixed composition there exists a critical velocity below which the growth of lamellae is favored. Note that this also implies that the transition can happen both ways, from rods to lamellae or from lamellae to rods, for decreasing and increasing velocity, respectively. It can also be triggered by a change in tilt angle.

Since the alloy phase diagram and the control parameters differ between experiments and simulations, these results indicate that this scenario is generic. For a more quantitative understanding, it is necessary to obtain more information on the propagative instability of lamellae as a function of lamellar spacing, volume fraction, and pulling velocity. It should be mentioned that this instability is clearly distinct from the Rayleigh–Plateau instability of a liquid jet [37] or diffusive instabilities of one-dimensional solid structures [38], since these instabilities do not have a threshold: a liquid jet or a solid cylinder is always unstable under the action of capillarity. In contrast, eutectic lamellae are stable for extended composition and velocity ranges. Furthermore, the transition might also be influenced by crystallographic effects (interface anisotropy), as recently evidenced for example in Ref. [39]. Phase-field simulations are clearly a promising tool to obtain more data on these questions.

An interesting perspective for experiments in microgravity would be to solidify a sample in which the liquid composition varies in space; this could be achieved by melting a solid sample that contains a carefully prepared concentration gradient. While this would be a "one-shot experiment" because the concentration gradient would decrease in the course of the experiment by diffusion in the liquid, it could still provide valuable insights on the lamella-to-rod transition since in this setting the transition occurs on a shorter time scale than in the experiments described here. Preparations for this kind of experiment are currently ongoing.

Conflicts of interest

The authors declare no competing financial interest.

Dedication

The manuscript was written through contributions of all authors. All authors have given approval to the final version of the manuscript.

Acknowledgments

References

[1] M. E. Glicksman, M. B. Koss, E. A. Winsa, "Dendritic Growth Velocities in Microgravity", *Phys. Rev. Lett.* **73** (1994), no. 4, p. 573-576.

[2] L. A. Tennenhouse, M. B. Koss, J. C. LaCombe, M. E. Glicksman, "Use of microgravity to interpret dendritic growth kinetics at small supercoolings", *J. Cryst. Growth* **174** (1997), p. 82-89, 10th American Conference on Crystal Growth/9th International Conference on Vapor Growth and Epitaxy, VAIL, CO, AUG 04-09, 1996.

[3] J. C. LaCombe, M. B. Koss, V. E. Fradkov, M. E. Glicksman, "Three-dimensional dendrite-tip morphology", *Phys. Rev. E* **52** (1995), no. 3, p. 2778-2786.

[4] M. B. Koss, J. C. LaCombe, L. A. Tennenhouse, M. E. Glicksman, E. A. Winsa, "Dendritic growth tip velocities and radii of curvature in microgravity", *Metall. Mater. Trans. A* **30** (1999), p. 3177-3190.

[5] J. J. Favier, J. P. Garandet, A. Rouzaud, D. Camel, "Mass-transport phenomena during solidification in microgravity – Preliminary results of the 1st MEPHISTO flight experiment", *J. Cryst. Growth* **140** (1994), p. 237-243.

[6] B. Drevet, H. Nguyen-Thi, D. Camel, B. Billia, M. D. Dupouy, "Solidification of aluminium-lithium alloys near the cell/dendrite transition-influence of solutal convection", *J. Cryst. Growth* **218** (2000), no. 4-5, p. 419-433.

[7] D. J. Jarvis, O. Minster, "Metallurgy in space", in *Solidification and Gravity IV* (R. Roósz, M. Rettenmayr, Z. G'ácsi, eds.), Materials Science Forum, vol. 508, Univ Miskolc, Mat & Met Engn Fac, Phys Met & Metalforming Dept; Hungarian Acad Sci, Res Grp Mat Sci; NASA MSFC; HAS, Mickolc Comm; Hungarian Space Off; Assoc Hungarian Foundries, Trans Tech Publications, 2006, 4$^{\text{th}}$ International Conference on Solidification and Gravity, Miskolc Lillafured, HUNGARY, SEP 06-09, 2004, p. 1-18.

[8] J. P. Garandet, G. Boutet, P. Lehmann, B. Drevet, D. Camel, A. Rouzaud, J. J. Favier, G. Faivre, S. Coriell, J. I. D. Alexander, B. Billia, "Morphological stability of a solid-liquid interface and cellular growth: Insights from thermoelectric measurements in microgravity experiments", *J. Cryst. Growth* **279** (2005), no. 1-2, p. 195-205.

[9] N. Bergeon, D. Tourret, L. Chen, J.-M. Debierre, R. Guérin, A. Ramirez, B. Billia, A. Karma, R. Trivedi, "Spatiotemporal Dynamics of Oscillatory Cellular Patterns in Three-Dimensional Directional Solidification", *Phys. Rev. Lett.* **110** (2013), article no. 226102.

[10] D. Tourret, J.-M. Debierre, Y. Song, F. L. Mota, N. Bergeon, R. Guérin, R. Trivedi, B. Billia, A. Karma, "Oscillatory cellular patterns in three-dimensional directional solidification", *Phys. Rev. E* **92** (2015), no. 4, article no. 042401.

[11] G. Salloum-Abou-Jaoude, H. Nguyen-Thi, G. Reinhart, R. H. Mathiesen, G. Zimmermann, D. Voss, "Characterization of Motion of Dendrite Fragment by X-Ray Radiography on Earth and under Microgravity Environment", *Materials Science Forum* **790-791** (2014), p. 311-316.

[12] M. Plapp, S. Bottin-Rousseau, G. Faivre, S. Akamatsu, "Eutectic solidification patterns: Interest of microgravity environment", *Comptes Rendus Mécanique* **345** (2017), no. 1, p. 56-65, Basic and applied researches in microgravity – A tribute to Bernard Zappoli's contribution.

[13] M. Plapp, M. Dejmek, "Stability of hexagonal solidification patterns", *Eur. Phys. Lett.* **65** (2004), no. 2, p. 276-282.

[14] K. A. Jackson, J. D. Hunt, "Lamellar and Rod Eutectic Growth", *Transactions of the Metallurgical Society of AIME* **236** (1966), p. 1129-1142.

[15] K. Kassner, C. Misbah, "Similarity laws in eutectic growth", *Phys. Rev. Lett.* **66** (1991), no. 4, p. 445-448.

[16] K. Kassner, C. Misbah, "Spontaneous parity-breaking transition in directional growth of lamellar eutectic structures", *Phys. Rev. A* **44** (1991), no. 10, p. 6533-6543.

[17] A. Karma, A. Sarkissian, "Morphological instabilities of lamellar eutectics", *Metall. Mater. Trans. A* **27** (1996), p. 635-656.

[18] M. Ginibre, S. Akamatsu, G. Faivre, "Experimental determination of the stability diagram of a lamellar eutectic growth front", *Phys. Rev. E* **56** (1997), p. 780-796.

[19] A. Parisi, M. Plapp, "Stability of lamellar eutectic growth", *Acta Mater.* **56** (2008), no. 6, p. 1348-1357.

[20] A. Parisi, M. Plapp, "Defects and multistability in eutectic solidification patterns", *Europhysics Letters* **90** (2010), article no. 26010.

[21] S. Liu, J. H. Lee, R. Trivedi, "Dynamic effects in the lamellar-rod eutectic transition", *Acta Mater.* **59** (2011), no. 8, p. 3102-3115.

[22] S. Bottin-Rousseau, V. T. Witusiewicz, U. Hecht, J. Fernandez, A. Laveron-Simavilla, S. Akamatsu, "Coexistence of rod-like and lamellar eutectic growth patterns", *Scr. Mater.* **207** (2022), article no. 114314.

[23] M. Şerefoğlu, S. Bottin-Rousseau, S. Akamatsu, "Lamella-rod pattern transition and confinement effects during eutectic growth", *Acta Mater.* **242** (2023), article no. 118425.

[24] M. Perrut, A. Parisi, S. Akamatsu, S. Bottin-Rousseau, G. Faivre, M. Plapp, "Role of transverse temperature gradients in the generation of lamellar eutectic solidification patterns", *Acta Mater.* **58** (2010), no. 5, p. 1761-1769.

[25] V. T. Witusiewicz, L. Sturz, U. Hecht, S. Rex, "Thermodynamic description and unidirectional solidification of eutectic organic alloys: I. Succinonitrile-(D)camphor system", *Acta Mater.* **52** (2004), p. 4561-4571.

[26] M. Şerefoğlu, R. E. Napolitano, "On the selection of rod-type eutectic morphologies: Geometrical constraint and array orientation", *Acta Mater.* **56** (2008), no. 15, p. 3862-3873.

[27] S. Akamatsu, S. Bottin-Rousseau, M. Perrut, G. Faivre, V. T. Witusiewicz, L. Sturz, "Real-time study of thin and bulk eutectic growth in succinonitrile-(D)camphor alloys", *J. Cryst. Growth* **299** (2007), no. 2, p. 418-428.

[28] M. Perrut, S. Akamatsu, S. Bottin-Rousseau, G. Faivre, "Long-time dynamics of the directional solidification of rodlike eutectics", *Phys. Rev. E* **79** (2009), no. 3, article no. 032602.

[29] M. Perrut, S. Bottin-Rousseau, G. Faivre, S. Akamatsu, "Dynamic instabilities of rod-like eutectic growth patterns: A real-time study", *Acta Mater.* **61** (2013), p. 6802-6808.

[30] S. Bottin-Rousseau, M. Perrut, C. Picard, S. Akamatsu, G. Faivre, "An experimental method for the in situ observation of eutectic growth patterns in bulk samples of transparent alloys", *J. Cryst. Growth* **306** (2007), p. 465-472.

[31] V. Trnovcová, P. P. Fedorov, C. Bàrta, V. Labas, V. A. Meleshina, B. P. Sobolev, "Microstructure and physical properties of superionic eutectic composites of the $LiF–RF_3$ (R 5 rare earth element) system", *Solid State Ionics* **119** (1999), no. 1-4, p. 173-180.

[32] M. Neuroth, K. Recker, F. Wallrafen, "Investigations on the directional solidification of the eutectic $LiF–LiBaF_3$", *Zeitschrift für Kristallographie - Crystalline Materials* **209** (1994), no. 4, p. 295-302.

[33] M. Şerefoğlu, S. Bottin-Rousseau, S. Akamatsu, G. Faivre, "Dynamics of rod eutectic growth patterns in confined geometry", in *The 3rd International Conference on Advances in Solidification Processes 7–10 June 2011, Rolduc Abbey, Aachen, The Netherlands*, IOP Conference Series: Materials Science and Engineering, vol. 27, IOP Science, 2012.

[34] R. Folch, M. Plapp, "Quantitative phase-field modeling of two-phase solidification", *Phys. Rev. E* **72** (2005), no. 1, article no. 011602.

[35] M. Şerefoğlu, R. E. Napolitano, M. Plapp, "Phase-field investigation of rod eutectic morphologies under geometrical confinement", *Phys. Rev. E* **84** (2011), article no. 011614.

[36] S. Akamatsu, S. Bottin-Rousseau, G. Faivre, "Experimental evidence for a zigzag bifurcation in bulk lamellar eutectic growth", *Phys. Rev. Lett.* **93** (2004), no. 17, article no. 175701.

[37] L. Rayleigh, "Instability of Jets", *Philos. Mag.* **36** (1878), p. 4.

[38] F. A. Nichols, W. W. Mullins, "Surface-(Interface-) and volume-diffusion contributions to morphological changes driven by capillarity", *Transactions of the Metallurgical Society of AIME* **233** (1965), no. 10, p. 1840-1848.

[39] S. Khanna, S. K. Aramanda, A. Choudhury, "Role of Solid–Solid Interfacial Energy Anisotropy in the Formation of Broken Lamellar Structures in Eutectic Systems", *Metall. Mater. Trans. A* **51** (2020), p. 6327-6345.